



Double-activated porous carbons for high-performance supercapacitor electrodes

Jing Sun, Shu-Hua Yang, Shan-Shan Li, Bing-Qiang Cao* 

Received: 13 December 2016/Revised: 2 February 2017/Accepted: 7 March 2017/Published online: 31 March 2017
© The Nonferrous Metals Society of China and Springer-Verlag Berlin Heidelberg 2017

Abstract The double-activated porous carbons (DAPCs) with unique bimodal pore structure were prepared by activating commercial microporous carbon (CMCs) twice through KOH (double activation) at high temperature. The as-prepared DAPCs show larger surface area ($833 \text{ m}^2 \cdot \text{g}^{-1}$), and the pores are composed of micropores (size of $\sim 1.8 \text{ nm}$) and mesopores (size of $\sim 4.5 \text{ nm}$). Such special hierarchical porous structures integrate the dual advantages of micropore and mesopore, having not only the high energy storage of the micropores but also the high-rate performance of the mesopores for supercapacitors (SCs). As a result, the optimized DAPCs-3-1 exhibits a high specific capacitance of $277 \text{ F} \cdot \text{g}^{-1}$ at $1 \text{ A} \cdot \text{g}^{-1}$, enhanced rate performance of $197 \text{ F} \cdot \text{g}^{-1}$ at a high current density of $10 \text{ A} \cdot \text{g}^{-1}$, and excellent cycling stability with 94.2% capacity retention after 10,000 cycles in the $1 \text{ mol} \cdot \text{L}^{-1}$ Na_2SO_4 electrolyte. The facile double activation could be a promising method to prepare suitable porous carbons with exceptional electrochemical properties for SCs.

Keywords Double activation; Activated carbon; Hierarchically porous carbons; Supercapacitor

1 Introduction

In recent years, carbon-based materials such as carbon nanoparticles [1–3], carbon nanotubes [4–6], graphene [7–9] have attracted intensive attention in fields of electrode

materials for supercapacitors (SCs) because of their unique advantages, including high specific surface area (SSA), good electrical and mechanical properties, and porous structure [10–15]. In particular, activated carbons (ACs) generally exhibit very good electrochemical performance in this application. However, conventional activated carbon materials have narrow microporous channels which lead to the sluggish ion transport and low capacitance retention at high charge–discharge rates [16, 17]. In addition, the pore structure of activated carbon also affects the performance of the capacitors obviously.

To overcome these issues and further improve the electrochemical performance of ACs, it is extremely necessary to develop novel ACs with large specific surface area and suitable pore size distribution [18–21]. In general, the electrochemical performance of ACs depends on not only the high specific surface area but also on the pore size distribution and architectures. It has been demonstrated that micropores ($<2 \text{ nm}$) are primarily responsible for the capacitance, while large pores or channels such as mesopores (2–50 nm) and macropores ($>50 \text{ nm}$) are associated with high-rate capacitive performance [22–25]. For example, Kang et al. [22] has fabricated porous carbon with small mesopores with size of 2–4 nm by using “egg-box” model, which shows high specific capacitance and excellent high-rate capacitive performance. Wei et al. [26] reported functional hierarchically porous carbons (HPCs) prepared from poly-N-phenylethanolamine and polyaniline conducting polymers through pyrolysis, chemical activation, and oxidation processes and studied their electrochemical behavior for SCs. It exhibits a high specific capacitance of $370 \text{ F} \cdot \text{g}^{-1}$ at $0.5 \text{ A} \cdot \text{g}^{-1}$ and good cycle durability, resulting from an appropriate selection of the surface chemistry, a reasonable pore size distribution, and a

J. Sun, S.-H. Yang, S.-S. Li, B.-Q. Cao*
Materials Center for Energy and Photoelectrochemical
Conversion, School of Material Science and Engineering,
University of Jinan, Jinan 250022, China
e-mail: mse_caobq@ujn.edu.cn

moderate Brunauer–Emmett–Teller (BET) surface area. Thus, HPCs with optimized pore size distribution are highly desired for high-performance SCs. Despite the previous listed advantages of HPCs [27], optimized pore architectures are still difficult to efficiently achieve.

To date, a template-assisted method is one of the promising methods for preparation and synthesis of the HPCs. However, the process of synthesis of HPCs materials by template-assisted method is very fussy, and the condition of experiment is so harsh [28, 29], which hinders the further development of HPCs with optimized pore structures for SCs. Therefore, it is imperative to develop a facile, cost-effective, and tailored synthesis strategy for the fabrication of HPCs with superior electrochemical performance, which can not only boost the energy density but also improve the kinetic process of ion diffusion and enhance the power density.

Herein, a facile and efficient double-activation strategy which is activating commercial microporous carbons (CMCs) twice through KOH at high temperature was reported for constructing a well-tailored porous carbon with optimized bimodal pore size distribution, exhibiting high specific capacitance and rate capability. As for such double-activated porous carbons (DAPCs), optimized bimodal pore size distribution is not only the high energy storage of the micropore but also the high-rate performance of the mesopore for SCs. As a result, the optimized DAPCs exhibit a high specific capacitance, enhanced rate performance and excellent cycling stability.

2 Experimental

2.1 Preparation of double-activated porous carbons

The commercial microporous carbons (CMCs) were obtained from Shanghai Lingfeng Chemical Reagent Co., Ltd, China. The first activated porous carbon (FAPC) was prepared by the KOH activation firstly. Typically, the CMCs and KOH were mixed in a mass ratio ranging from 4:1 to 1:2, and then the mixtures were ground uniformly in an agate mortar. The obtained mixtures were put into a horizontal tube furnace and heated at 600 °C for 2 h under an argon flow of 600 ml·min⁻¹. The temperature was ramped from room temperature to 600 °C at a heating rate of 5 °C·min⁻¹. The obtained samples were washed thoroughly with 5 mol·L⁻¹ hydrochloric acid and deionized water until pH 7. The producing samples were named as FAPCs-4-1, FAPCs-3-1, FAPCs-2-1, FAPCs-1-1, and FAPCs-1-2 corresponding to the CMCs and KOH mass ratio ranging from 4:1 to 1:2. Optimal FAPCs (FAPCs-2-1) were selected, and a series of similar experiments were

carried out to prepare the double-activated porous carbons (DAPCs). The obtained samples were denoted as DAPCs-4-1, DAPCs-3-1, DAPCs-2-1, DAPCs-1-1, and DAPCs-1-2.

2.2 Material characterization

The FAPCs-2-1 and DAPCs-3-1 were analyzed by scanning electron microscope (SEM, FE-SEM, Quanta 250, FEI) and transmission electron microscope (TEM, JEM-2100F, JEOL) observations. Pore structures were characterized using N₂ adsorption–desorption at 77.4 K, (ASAP 2020). The SSA of the samples was calculated using BET method with a p/p_0 (p is partial pressure of the nitrogen and p_0 is saturated vapor pressure of the nitrogen at the temperature of the liquid nitrogen) value between 0.1 and 1.0 with N₂ adsorption data. The average micropore size and mesopore size were determined by the density functional theory (DFT) method. Before all the gas adsorption measurements, the samples were degassed at 150 °C for 4 h.

2.3 Electrochemical characterization

All the samples were tested by a three-electrode system. The working electrodes were fabricated as follows. The as-prepared materials were mixed with acetylene black and polyvinylidene difluoride (PVDF) with a weight ratio of 8:15:5 in N-methyl pyrrolidone (NMP) solvent. The resulting slurry was coated onto the nickel foam substrate (1 cm × 1 cm) with a spatula, followed by drying at 110 °C for 12 h. Finally, the electrode was pressed under a pressure of 10 MPa for 30 s. The mass load of each electrode plate was about 2.0 mg. All electrochemical measurements were carried out in 1 mol·L⁻¹ Na₂SO₄ electrolyte.

Cyclic voltammetry (CV), galvanostatic charge–discharge (GCD), and electrochemical impedance spectrum (EIS) were measured on an electrochemical station (Zennium, Zahner). The voltage window for aqueous electrolyte was set to be 0–1 V. The scan rate was in a range 5–200 mV·s⁻¹. GCD measurement was conducted under a current density ranging from 1 to 10 A·g⁻¹, and the voltage was set to 0–1.0 V for the aqueous system. EIS was collected with frequencies ranging from 100 kHz to 100 mHz with an alternative current (AC) amplitude of 5 mV.

The samples' gravimetric capacitance (C) was calculated from the GCD discharge curves, according to the following equation:

$$C = I\Delta t / \Delta V m \quad (1)$$

where I is the current, Δt denotes the discharging time, and ΔV is the voltage, respectively. In both cases, m is the mass load of the activated material on one electrode plate.

3 Results and discussion

The double-activation process and detailed structure of the DAPCs are schematically illustrated in Fig. 1. In the process of activation, the carbon/KOH reaction mechanism, according to the global reaction: $6\text{KOH} + \text{C} \leftrightarrow 2\text{K} + 3\text{H}_2 + 2\text{K}_2\text{CO}_3$, can effectively develop micropores for different kinds of ACs [30–32]. The CMCs were firstly activated with KOH, producing the first activated porous carbons (FAPCs) with unimodal micropores. The optimized FAPCs (FAPCs-2-1) were activated by KOH again, obtaining the DAPCs with bimodal pore structure (micropores and mesopores). During the second KOH activation, KOH inside the micropores not only has pore-reaming effect, but also creates a huge number of new micropores in the original pore wall under the thermal annealing, leading to bimodal pore structure (micropores and mesopores). The generated mesopores provide affluent channels to transfer ion into the interior micropores for energy storage and effectively increase the ion transport rate. Compared to FAPCs, the obtained DAPCs offer high ion-accessible micropores, large specific surface area, and affluent channels for ions to transport into interior micropores. Therefore, an excellent electrochemical behavior with a high specific capacitance and high-rate performance has been

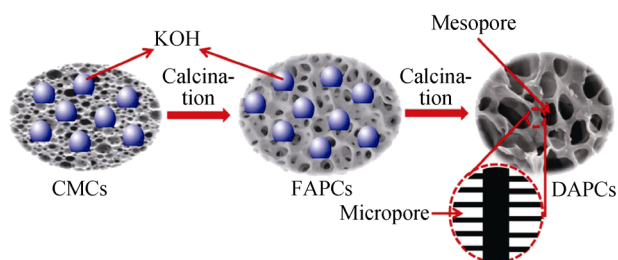


Fig. 1 Illustration of formation of DAPCs with bimodal pore structure

obtained, indicating that the double-activation strategy reported here is effective for constructing optimized pore architectures for energy storage.

The FAPCs (DAPCs) with different mass ratios of CMCs (FAPCs) and KOH were synthesized. The optimized products (FAPCs-2-1 and DAPCs-3-1) were selected and discussed below (Fig. 2a, b). The morphologies of as-prepared FAPCs-2-1 and DAPCs-3-1 were examined by SEM and TEM. Compared with that of FAPCs-2-1 (Fig. 3a–d), the texture of DAPCs-3-1 (Fig. 3e–h) is rougher due to the producing mesopores [33]. In the double-activation process, the FAPCs can provide a larger accessible surface area for active agents (KOH) than CMCs. Thus, the DAPCs have a large amount of micropores and affluent mesopores, which could improve charge store and ion transport simultaneously for SCs. The microstructures of FAPCs-2-1 and DAPCs-3-1 are further confirmed by the low-magnification TEM image and HRTEM (Fig. 4). Clearly, FAPCs-2-1 is mainly composed of micropores, whereas DAPCs-3-1 contains micropores and mesopores. Distorted lattice fringes are visible throughout both samples, indicating a partial graphitization texture. It has been demonstrated that such graphitized texture can provide excellent conductivity.

The specific surface area and pore size distribution of FAPCs-2-1 and DAPCs-3-1 were characterized using N_2 adsorption/desorption (77.4 K) measurements. The N_2 isotherms of FAPCs-2-1 and DAPCs-3-1 (Fig. 5) reveal the details of various N_2 adsorption/desorption stages. For both FAPCs-2-1 and DAPCs-3-1 samples, the micropore filling occurs at the low-pressure region, indicating the presence of micropores. However, the hysteresis loops at high pressure range are more pronounced for DAPCs-3-1, which suggests the formation of mesopores [34–36]. The specific surface areas of FAPCs-2-1 and DAPCs-3-1 calculated using Brunauer–Emmett–Teller (BET) method (S_{BET}) are 652 and 833 $\text{m}^2\cdot\text{g}^{-1}$ (Table 1, where V_{mic} is the volume of

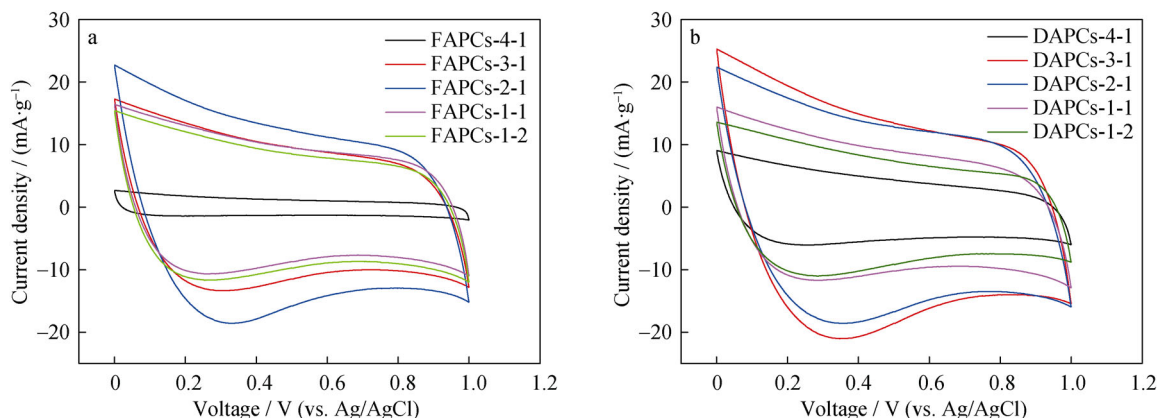


Fig. 2 **a** CV curves of **a** FAPCs-4-1, FAPCs-3-1, FAPCs-2-1, FAPCs-1-1, and FAPCs-1-2 at voltage scan rate of $100\text{ mV}\cdot\text{s}^{-1}$ and **b** DAPCs-4-1, DAPCs-3-1, DAPCs-2-1, DAPCs-1-1, and DAPCs-1-2 at voltage scan rate of $100\text{ mV}\cdot\text{s}^{-1}$

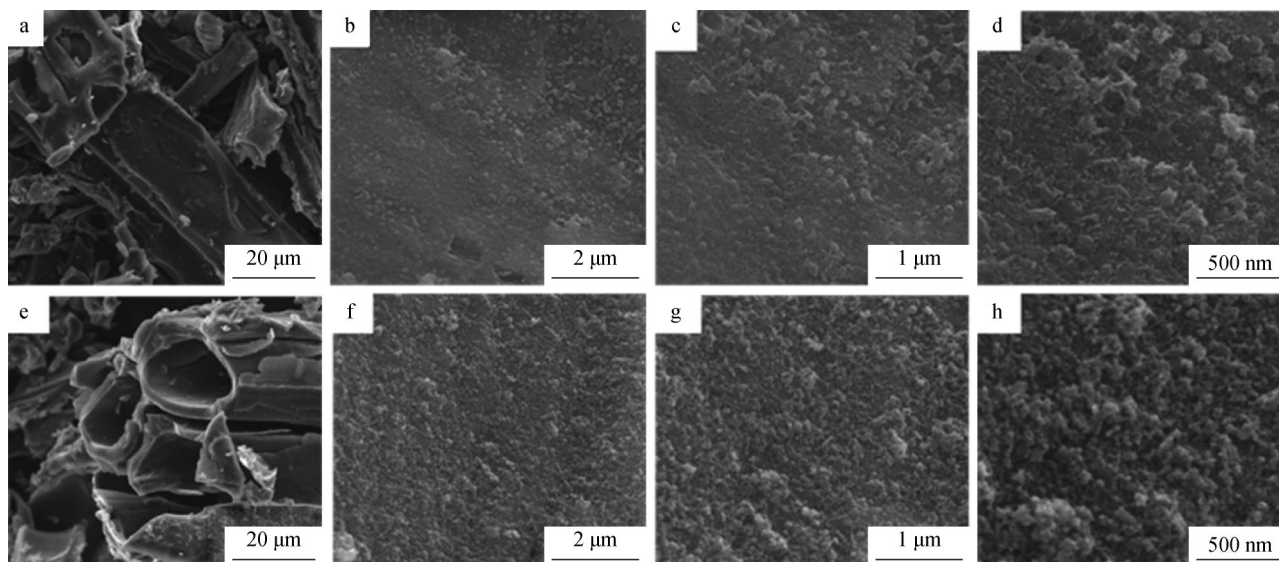


Fig. 3 SEM images of samples: **a–d** FAPCs-2-1 and **e–h** DAPCs-3-1

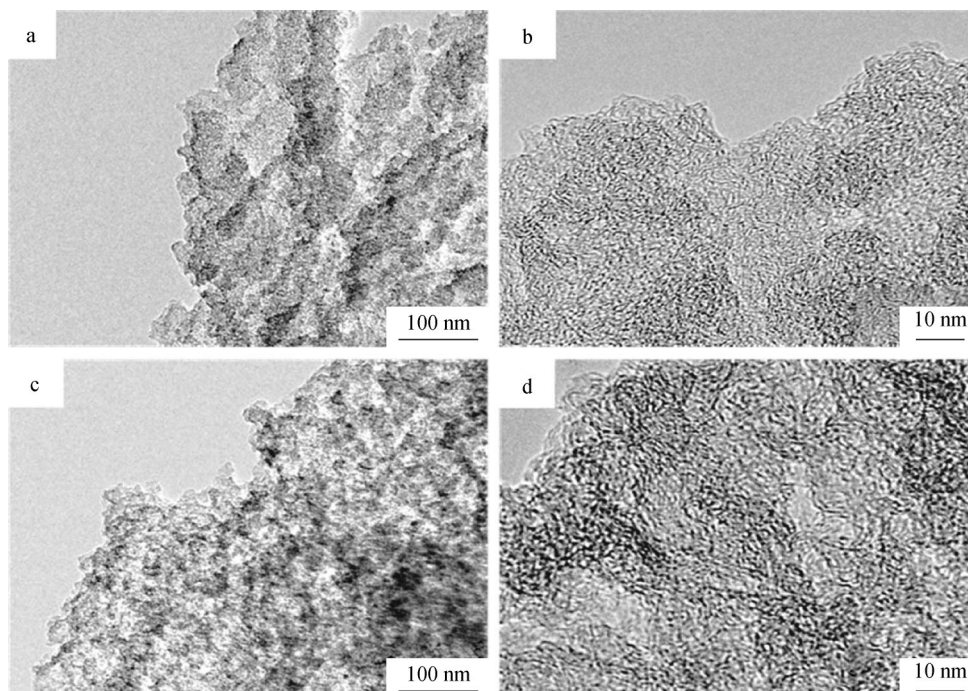


Fig. 4 TEM images of samples: **a, b** FAPCs-2-1 and **c, d** DAPCs-3-1

micropores), respectively, indicating that the double-activation process greatly increases the specific surface area due to the creation of additional pores and widening of micropores. Apart from surface area, pore size distribution was determined by density functional theory (DET) method using adsorption data (Fig. 5b). As expected, pore size distribution of FAPCs-2-1 falls in the micropores range. And DAPCs-3-1 exhibits two distinct peaks at 1.8 and 4.5 nm which lie in the microporous and mesoporous

range, respectively. It is well known that the presence of such small mesopores will enhance the supercapacitive behavior of the carbonaceous electrode [33, 37]. Therefore, enhanced electrochemical performance is expected for DAPCs, resulting from a large accessible surface area for energy storage and affluent mesopores for ion transport.

The electrochemical performance of FAPCs-2-1 and DAPCs-3-1 were studied by CV and GCD measurements in three-electrode system with $1 \text{ mol} \cdot \text{L}^{-1} \text{ Na}_2\text{SO}_4$

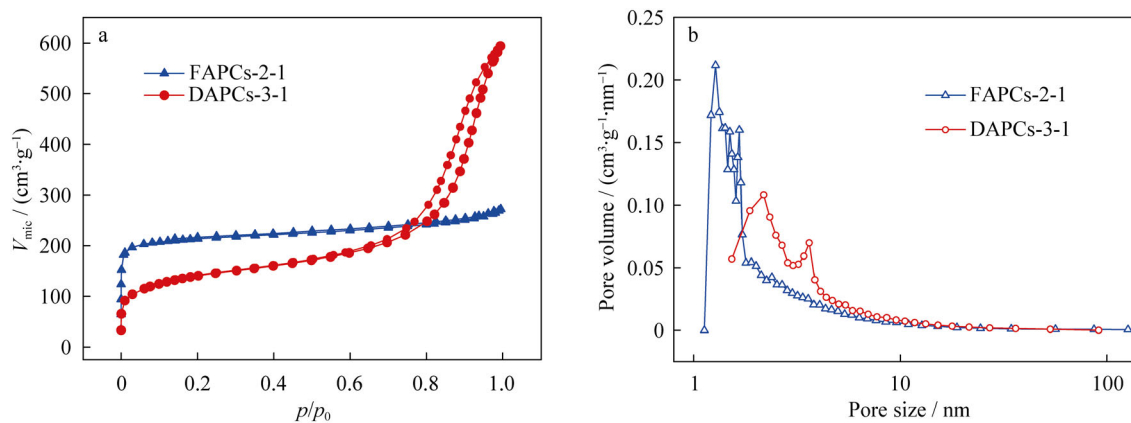


Fig. 5 Nitrogen adsorption isotherms of FAPCs-2-1 and DAPCs-3-1 **a** and pore size distribution of FAPCs-2-1 and DAPCs-3-1 using DFT model **b**

Table 1 Characteristics of pores in CACs, FAPCs-2-1, and DAPCs-3-1

Samples	$S_{BET}/(m^2 \cdot g^{-1})$	Diameter/nm		$V_{mic}/(cm^3 \cdot g^{-1})$
		Micropore	Mesopore	
FAPCs-2-1	652	1.1	–	0.288
DAPCs-3-1	833	1.8	4.5	0.331

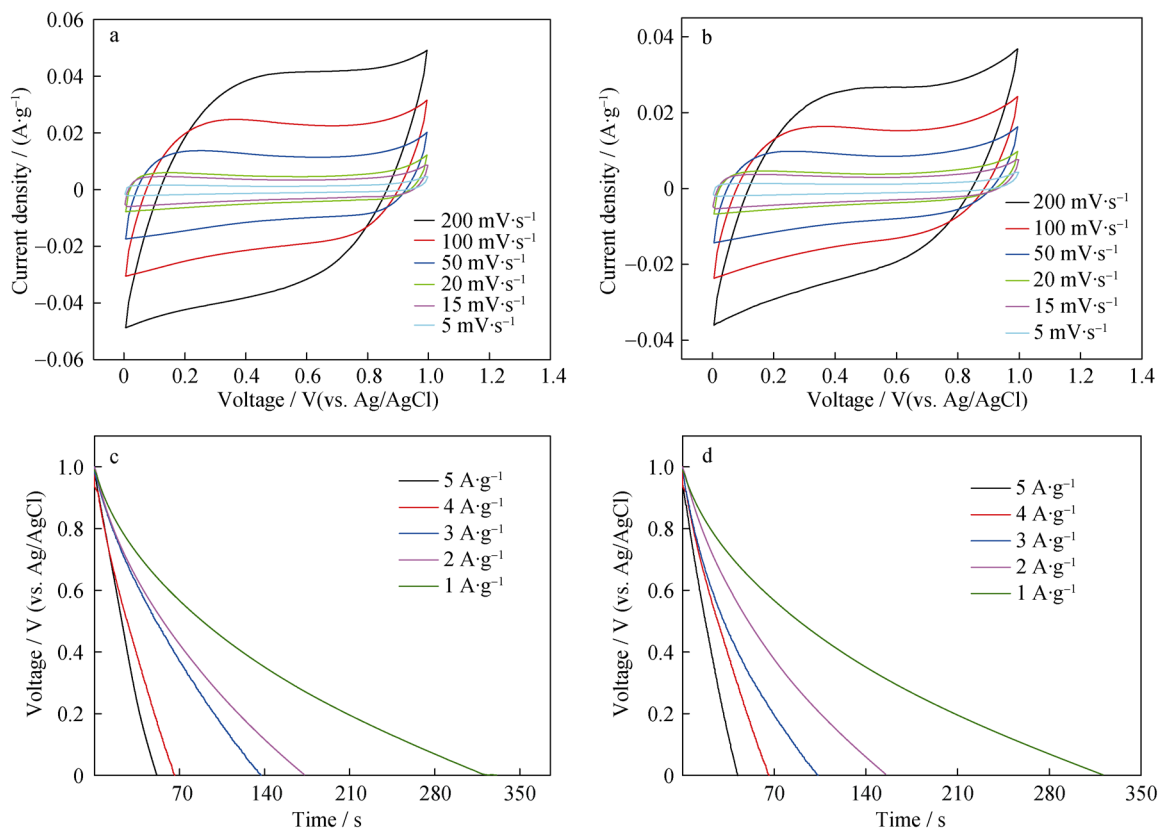


Fig. 6 CV curves of **a** DAPCs-3-1 and **b** FAPCs-2-1 and GCD curves of **c** DAPCs-3-1 and **d** FAPCs-2-1

electrolyte. The CV curves of DAPCs-3-1 show rectangular shape from 0 to 1 V at a wide range of voltage scan rates (Fig. 6a), implying an ideal electric double-layer performance. A negligible small shape distortion in CV curves is observed for DAPCs-3-1 as the scan rate increases from 5 to 200 $\text{mV}\cdot\text{s}^{-1}$, indicating the strong ion transport ability of the hierarchical pore structure from the double-activation. The CV curves of FAPCs-2-1 (Fig. 6b) are similar to a rectangle. However, the CV curves of FAPCs-2-1 have an obvious polarization phenomenon, and the symmetry is lower than that of DAPCs-3-1, which indicates that DAPCs-3-1 possesses much better electron and ion transfer rate. The discharge curves of DAPCs-3-1

electrode at different charge/discharge currents are shown in Fig. 6c. The voltage drop is negligible, demonstrating high conductivity of DAPCs-3-1 due to the increasing graphitization by double activation. The capacitance values of DAPCs-3-1 calculated from discharge curves are 277, 268, 258, 246, and 238 $\text{F}\cdot\text{g}^{-1}$ at a current density of 1, 2, 3, 4, and 5 $\text{A}\cdot\text{g}^{-1}$, respectively (Fig. 6c). By contrast, the shorter discharging time of FAPCs-2-1 (Fig. 6d) represents the lower capacitance than DAPCs-3-1, indicating that the capacitance values of DAPCs-3-1 are significantly higher than those of FAPCs-2-1, which further demonstrate that DAPCs-3-1 has higher store energy.

The specific capacitance versus current density for FAPCs-2-1 and DAPCs-3-1 electrodes are shown in Fig. 7. It can be seen that the specific capacitance of FAPCs-2-1 decays fast as the current density increases. In contrast, DAPCs-3-1 shows excellent rate performance ($197 \text{ F}\cdot\text{g}^{-1}$) at high rate ($10 \text{ A}\cdot\text{g}^{-1}$), resulting from affluent mesopores as ion channels. The Nyquist plots of FAPCs-2-1 and DAPCs-3-1 illustrate vertical curves at low frequencies (Fig. 8a), indicating an ideal capacitive behavior of electrode materials. Compared with that of FAPCs-2-1, the curve of DAPCs-3-1 is more vertical due to the abundant mesopores generated by double-activation, which is conducive to the rapid transport of electrolyte ions in the electrode. In high frequencies, the intersection of semicircle and x -axis in Fig. 8a represents the equivalent series resistance (ESR), which is 2.17 and 1.76 Ω , respectively. In addition, the ZSimpWin software was used to simulate

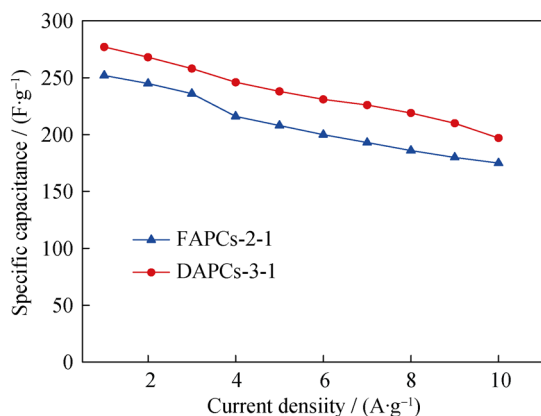


Fig. 7 Capacitance retention versus current density of FAPCs-2-1 and DAPCs-3-1

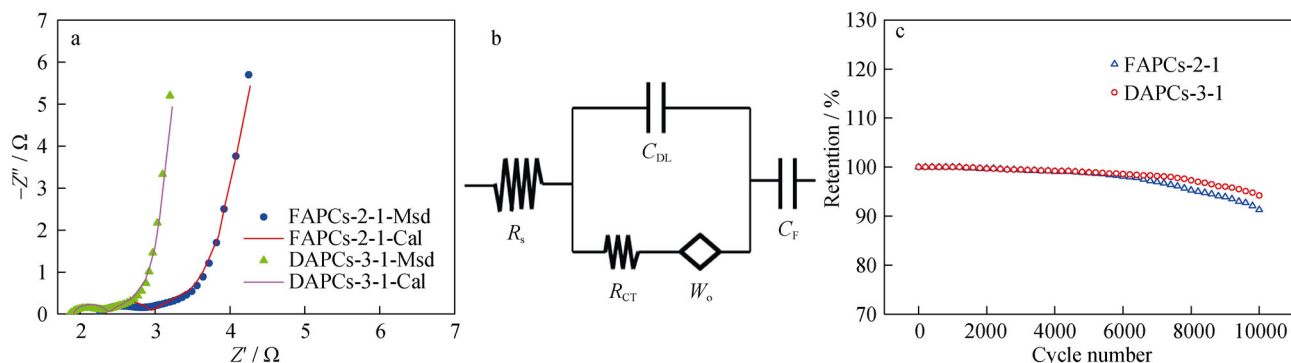


Fig. 8 Nyquist plots for FAPCs-2-1-Msd, FAPCs-2-1-Cal, DAPCs-3-1-Msd, and DAPCs-3-1-Cal **a**, equivalent circuit model **b**, and cyclic stability of FAPCs-2-1 and DAPCs-3-1 in $1 \text{ mol}\cdot\text{L}^{-1} \text{ Na}_2\text{SO}_4$ electrolyte at a current density of $1 \text{ A}\cdot\text{g}^{-1}$ **c**

Table 2 Parameters of equivalent circuit for different electrodes

Samples	R_s/Ω		R_{CT}/Ω	W_o/Ω	C_{DL}/F	$C_F/(10^{-4} \text{ F})$
	Measured	Calculated				
FAPCs-2-1	2.17	2.197	0.5782	0.4781	0.4468	1.356
DAPCs-3-1	1.76	1.816	0.4042	0.3274	0.4359	1.389

the EIS of FAPCs-2-1 and DAPCs-3-1, and the equivalent circuit model and the simulated results are shown in Fig. 8a, b and Table 2. Both the measured and calculated EIS data match well with each other using the equivalent circuit model. R_s which represents the equivalent series resistance (ESR) is obtained from the intercepts in the Nyquist plot, corresponding to the electrolyte resistance, the internal resistance of the electrode, and the contact resistance. The semicircular behavior in the high- to mid-frequency region corresponds to the parallel connection of the interfacial charge transfer resistance (R_{CT}) and the double-layer capacitance (C_{DL}). And W_o is the finite-length Warburg diffusion element [38–40]. The ESR of DAPCs-3-1 is significantly reduced, indicating better conductivity of DAPCs-3-1 due to the increasing graphitization, which is consistent with the results of GCD measurements. Cycling performance of FAPCs-2-1 and DAPCs-3-1 was conducted at a current density of $1 \text{ A}\cdot\text{g}^{-1}$ for 10,000 cycles in $1 \text{ mol}\cdot\text{L}^{-1} \text{ Na}_2\text{SO}_4$. As shown in Fig. 8c, there is nearly no capacitance fading after 5000 cycles, and the capacitance retention is 94.2% after 10,000 cycles, but the capacitance retention of FAPCs-2-1 is 91.3% after 10,000 cycles, indicating that DAPCs-3-1 has superior stable cycle stability.

The high capacitance, excellent rate capability, and good cycle performance delivered by DAPCs-3-1 electrode can be elucidated by unique bimodal pore structure and high graphitization. DAPCs-3-1 electrode not only stores high energy by micropores but also provides affluent mesopores as ion transport channel. In addition, the double-activation can effectively improve the conductivity of CMCs electrode. All of the above results clearly demonstrate that the as-developed DAPCs-3-1 by double-activation method has significantly improved electrochemical performance compared with FAPCs-2-1 generated by single activation.

4 Conclusion

A facile and efficient double-activation strategy was developed to prepare the DAPCs with bimodal pore structure. The as-prepared DAPCs show larger surface area ($833 \text{ m}^2\cdot\text{g}^{-1}$), in which the pores are composed of micropores (size $\sim 1.8 \text{ nm}$) and mesopores (size $\sim 4.5 \text{ nm}$). The mesopores can facilitate ion transfer, and the micropores can store high energy, so that the DAPCs-3-1 has a high specific capacitance of $277 \text{ F}\cdot\text{g}^{-1}$ at a current density of $1 \text{ A}\cdot\text{g}^{-1}$ and enhanced rate performance of $197 \text{ F}\cdot\text{g}^{-1}$ at a high current density of $10 \text{ A}\cdot\text{g}^{-1}$. Meanwhile, there is nearly no capacitance fading after 5000 cycles, and the capacitance retention is 94.2% after 10,000 cycles.

Acknowledgments This work was financially supported by the National Natural Science Foundation of China (No. 51472110), Shandong Provincial Natural Science Foundation (No. ZR2016EMB05), University of Jinan Science Foundation (No. XKY1630), and a Research Project from Ministry of Education, China (No. 213021A).

References

- [1] Kumar VB, Borenstein A, Markovsky B, Aurbach D, Gedanken A, Talianker M, Porat Z. Activated carbon modified with carbon nanodots as novel electrode material for supercapacitors. *J Phys Chem C*. 2016;120(25):13406.
- [2] Faraji S, Ani FN. The development supercapacitor from activated carbon by electroless plating—a review. *Renew Sustain Energy Rev*. 2015;42:823.
- [3] Chen Q, Hu Y, Hu CG, Cheng HH, Zhang ZP, Shao HB, Qu LT. Graphene quantum dots-three-dimensional graphene composites for high-performance supercapacitors. *Phys Chem Chem Phys*. 2014;16(36):19307.
- [4] Tian YH. The development of supercapacitor with porous carbon materials. *J Power Sources*. 2002;26(6):466.
- [5] Yoo EJ, Kim J, Hosono E. Large reversible Li storage of graphene nanosheet families for use in rechargeable lithium ion batteries. *Nano Lett*. 2008;8(8):2277.
- [6] Yuan B, Zhou L, Guan DA. The development of supercapacitor with carbon-based electrode materials. *Mar Electr Eng*. 2016;36(1):33.
- [7] Kota M, Yu X, Yeon SH, Cheong HW, Park HS. Ice-templated three dimensional nitrogen doped graphene for enhanced supercapacitor performance. *J Power Sources*. 2016;303:372.
- [8] Zhang L, DeArmond D, Alvarez NT, Zhao D, Wang T, Hou G, Malik R, Heineman WR, Shanov V. Beyond graphene foam, a new form of three-dimensional graphene for supercapacitor electrodes. *J Mater Chem A*. 2016;4(9):1876.
- [9] Lamberti A, Clerici F, Fontana M, Scaltrito LA. Highly stretchable supercapacitor using laser-induced graphene electrodes onto elastomeric substrate. *Adv Energy Mater*. 2016;6(10):1600050.
- [10] Bose S, Kuila T, Mishra AK, Rajasekar R, Kim NH, Lee JH. Carbon-based nanostructured materials and their composites as supercapacitor electrodes. *J Mater Chem*. 2012;22(3):767.
- [11] Qiu YC, Li G, Hou Y, Pan Z, Li HF, Li WF, Liu MN, Ye FM, Yang XW, Zhang YG. Vertically aligned carbon nanotubes on carbon nanofibers: a hierarchical three-dimensional carbon nanostructure for high-energy flexible supercapacitors. *Chem Mater*. 2015;27(4):1194.
- [12] Park JW, Park SJ, Kwon OS, Lee C, Jang J, Jang J, Park JW, Park SJ, Lee C, Kwon OS. In situ synthesis of graphene/poly-selenophene nanohybrid materials as highly flexible energy storage electrodes. *Chem Mater*. 2014;26(7):2354.
- [13] Pierre AC, Pajonk GM. Chemistry of aerogels and their applications. *Chem Rev*. 2002;102(11):4243.
- [14] Moreno-Castilla C, Maldonado-Hódar FJ. Carbon aerogels for catalysis applications: an overview. *Carbon*. 2005;43(3):455.
- [15] Nardecchia S, Carriazo D, Ferrer ML, Gutierrez MC, del Monte F. Three dimensional macroporous architectures and aerogels built of carbon nanotubes and/or graphene: synthesis and applications. *Chem Soc Rev*. 2013;42(2):794.
- [16] Chen Z, Wen J, Yan CZ, Rice L, Sohn H, Shen MQ, Cai M, Dunn B, Lu YF. High-performance supercapacitors based on hierarchically porous graphite particles. *Adv Energy Mater*. 2011;1(4):551.

- [17] Mun Y, Jo C, Hyeon T, Lee J, Ha KS, Jun KW, Lee SH, Hong SW, Lee HI, Yoon S, Lee J. Simple synthesis of hierarchically structured partially graphitized carbon by emulsion/block-copolymer co-template method for high power supercapacitors. *Carbon*. 2013;64:391.
- [18] Ma C, Song Y, Shi JL, Zhang DQ, Zhai XL, Zhong M, Guo QG, Liu L. Preparation and one-step activation of microporous carbon nanofibers for use as supercapacitor electrodes. *Carbon*. 2013;51:290.
- [19] Lei Z, Christov N, Zhang LL, Zhao XS. Mesoporous carbon nanospheres with an excellent electrocapacitive performance. *J Mater Chem*. 2011;21(7):2274.
- [20] Dai L. Functionalization of graphene for efficient energy conversion and storage. *Acc Chem Res*. 2013;46(1):12.
- [21] Hu CG, Zhang YY, Bao G, Zhang YL, Liu ML, Wang ZL. Diameter-dependent voltammetric properties of carbon nanotubes. *Chem Phys Lett*. 2006;418(4):524.
- [22] Kang DM, Liu QL, Gu JJ, Su YS, Zhang W, Zhang D. "Egg-Box"-assisted fabrication of porous carbon with small mesopores for high-rate electric double layer capacitors. *ACS Nano*. 2015;9(11):11225.
- [23] Wang DW, Li F, Liu M, Lu GQ, Cheng HM. 3D aperiodic hierarchical porous graphitic carbon material for high-rate electrochemical capacitive energy storage. *Angew Chem*. 2007;120(2):379.
- [24] Wu ZS, Sun Y, Tan YZ, Yang S, Feng X, Müllen K. Three-dimensional graphene-based macro- and mesoporous frameworks for high-performance electrochemical capacitive energy storage. *J Am Chem Soc*. 2012;134(48):19532.
- [25] Chmiola J, Yushin G, Gogotsi Y, Portet C, Simon P, Taberna PL. Anomalous increase in carbon capacitance at pore sizes less than 1 nanometer. *Science*. 2006;313(5794):1760.
- [26] Wei XJ, Jiang XQ, Wei JS, Gao SY. Functional groups and pore size distribution do matter to hierarchically porous carbons as high-rate-performance supercapacitors. *Chem Mater*. 2016;28(2):445.
- [27] Li MC, Wang WX, Yang MY, Lv FC, Cao LJ, Tang YG, Sun R, Lu ZG. Large-scale fabrication of porous carbon decorated iron oxide microcuboids from Fe-MOF as high-performance anode materials for lithium-ion batteries. *RSC Adv*. 2015;5(10):7356.
- [28] Tao PP, Hu J, Wang WX, Wang S, Li MC, Zhong H, Tang YG, Lu ZG. Porous graphitic carbon prepared from the catalytic carbonization of Mo-containing resin for supercapacitors. *RSC Adv*. 2014;4(26):13518.
- [29] Hu J, Tao PP, Wang S, Liu Y, Tang YG, Zhong H, Lu ZG. Preparation of highly graphitized porous carbon from resins after the treatment of Cr⁶⁺-containing wastewater for supercapacitors. *J Mater Chem A*. 2013;1(22):6558.
- [30] Lillo-Ródenas MA, Juan-Juan J, Cazorla-Amorós D, Linares-Solano A. About reactions occurring during chemical activation with hydroxides. *Carbon*. 2004;42(7):1371.
- [31] Lillo-Rodenas MA, Cazorla-Amoros D, Linares-Solano A. Understanding chemical reactions between carbons and NaOH. *Carbon*. 2003;41(2):267.
- [32] Mckee DW. Gasification of graphite in carbon dioxide and water vapour—the catalytic effects of alkali metal salts. *Carbon*. 1982;20(1):59.
- [33] Jain A, Aravindan V, Jayaraman S, Kumar PS, Balasubramanian R, Ramakrishna S, Madhavi S, Srinivasan MP. Activated carbons derived from coconut shells as high energy density cathode material for Li-ion capacitors. *Sci Rep*. 2013;3:3002.
- [34] Carrot PJM, Roberts RA, Sing KSW. Adsorption of nitrogen by porous and non-porous carbons. *Carbon*. 1987;25(1):59.
- [35] Sing KS, Everett DH, Haul AW, Moscou L, Pierotti RA, Rouquerol J, Siemieniewska T. Physical and biophysical chemistry division commission on colloid and surface chemistry including catalysis. *Pure Appl Chem*. 1985;57(4):17.
- [36] Sing KSW, Everett DH, Haul AW, Moscou L, Pierotti RA, Rouquerol J, Siemieniewska T. Reporting physisorption data for gas solid systems with special reference to the determination of surface area and porosity. *Pure Appl Chem*. 1985;57(4):603.
- [37] Simon P, Gogotsi Y. Materials for electrochemical capacitors. *Nat Mater*. 2008;7(11):845.
- [38] Wang Q, Wen ZH, Li JH. A hybrid supercapacitor fabricated with a carbon nanotube cathode and a TiO₂-B nanowire anode. *Adv Funct Mater*. 2006;16(16):2141.
- [39] Qu GX, Cheng JL, Li XD, Yuan DM, Chen PN, Chen XL, Wang B, Peng HS. A fiber supercapacitor with high energy density based on hollow graphene/conducting polymer fiber electrode. *Adv Mater*. 2016;28(19):3646.
- [40] Choi BG, Hong J, Hong WH, Hammond PT, Park H. Facilitated ion transport in all-solid-state flexible supercapacitors. *ACS Nano*. 2011;5(9):7205.